Groundwater Responses to Recharge and Flood in Riparian Zones of Layered Aquifers: An Analytical Model

Jiangwei Zhang[1,3], Xiuyu Liang[1,2*], You-Kuan Zhang[1,4], Xiaohui Chen[3], Enze Ma[1], and Keith Schilling[4]

[1]School of Environmental Science and Engineering, Southern University of Science and Technology, Shenzhen, Guangdong 518055, P. R. China
[2]Shenzhen Key Laboratory of Natural Gas Hydrates, Southern University of Science and Technology, Shenzhen 518055, China.
[3]School of Civil Engineering, University of Leeds, Leeds, LS2 9JT, UK
[4]Department of Earth and Environmental Sciences, University of Iowa, Iowa City, IA 52242, U.S.A.

*Corresponding author: Xiuyu Liang (liangxy@sustech.edu.cn)

Manuscript submitted to ***Journal of Hydrology***

Abstract

A riparian zone is an important element in a river-aquifer system, controlling water exchange and other chemical and biological processes between a river and an aquifer. Complex groundwater flow patterns may occur due to aquifer heterogeneity within a riparian zone. The purpose of this study is to investigate the impacts of layered heterogeneity on water exchange in the riparian zone using a mathematical model for groundwater flow in a two-layer aquifer that is recharged by precipitation and floods. A semi-analytical solution is derived for the hydraulic head, lateral discharge, and fluxes between the layers. Results demonstrate that the hydraulic conductivity difference between the two layers enhances lateral flow in the higher permeable layer and, more importantly, generates vertical flow between the two layers. The vertical flow induced by the recharge event is downward while it could be upward or downward induced by the flood event, which is determined by the contrast in permeabilities of the two layers. Using an equivalent hydraulic conductivity approach underestimates discharge of the two-layer aquifer due to recharge or flood. The analytical solution closely matched the observed hydraulic heads in riparian zone well of White Clay Creek and provided reasonable estimates of aquifer parameters. The present solution provides a valuable basis for further study of chemical and biological processes in riparian zone.

Keywords: heterogeneity; unconfined aquifer; riparian zones; analytical solution.

1. Introduction

The riparian zone constitutes an important landscape element in a river-aquifer system due to its location in a catchment (Robert,1997; Webster,1976). It possesses a unique spatial structure and ecological function, and plays a significant role in regulating water quantity and quality exchanges in a river-aquifer system. For example, a riparian forest may reduce recharge from precipitation, or agricultural chemicals applied riparian crops may contaminate groundwater and river water (Gonzales-Inca et al., 2015; Krutz et al., 2005; Oliveira et al., 2010; Ou et al., 2016). The hyporheic zone within the riparian zone is defined by shallow subsurface pathways through river beds and river banks beginning and ending at the river (Boano et al., 2014) and this area is considered a hot spot for hydrologic, geologic, geomorphic, geochemical, and biological processes (Fox et al., 2016).

Groundwater flow is the controlling factor for many processes in the riparian and hyporheic zones, and it is greatly influenced by natural events and human activities. Flooding is one of the most important natural events affecting groundwater flow in the riparian and hyporheic zone, as rapid water level fluctuations give rise to lateral propagation of river water into the riparian zone that changes the local flow field (Curry et al. 1994; Liu et al. 2020). In addition, large-scale human activities (e.g., damming, river channelization, artificial flow regulation) can reduce the flood pulse of natural rivers and make the river level fluctuate more intermittently (Arias et al. 2013; Liu et al. 2020; Nilsson et al., 2000), which may substantially impact hydrologic exchange in the riparian zone (Fritz et al., 2007) and groundwater flow (Ferencz et al. 2019). Moreover, human society, especially coastal mega-cities, will face increasing flood risk under the current protection standard because of future climate change (Hu et al., 2019; Huang et al., 2020; Xu et al., 2022). Variable recharge from precipitation further impacts riparian zone hydrology

(Schilling et al., 2004), and it should be considered along with flooding to obtain a better understanding of the complex patterns of groundwater flow in the riparian zone.

Spatiotemporal responses to hydrological events with riparian or hyporheic zones and impacts on surface-groundwater exchanges have been investigated in extant literature (Chen et al., 2003; Hantush 2005; McCallum et al., 2016; Zlotnik et al., 1999). Singh (2004) considered stream boundary resistance and presented a 1-D analytical solution for semi-infinite aquifer responses to a sinusoidal river stage fluctuation. Liang et al. (2017b) developed a semi-analytical solution for base flow recession caused by recharge by considering lateral unsaturated discharge and aquifer compressibility. Their results showed that the unsaturated zone imparts a damping effect on the saturated flow. These studies, however, only considered groundwater flow in a cross section of a river-aquifer system. To explore the plane view of the surface-groundwater exchange, Liang et al. (2018) presented an analytical solution for the spatiotemporal response of horizontal 2-D groundwater flow in an unconfined aquifer, and surface water and groundwater exchanges due to a flood event. The results demonstrated that the 1-D cross-section aquifer-river model overestimates both the hydraulic head and discharge in the upstream aquifer, and underestimates the hydraulic head in the downstream aquifer, because it neglects groundwater flow parallel to the river channel.

One of the limitations in the above-mentioned studies is the assumption of the homogeneous condition. In fact, heterogeneity is intrinsic in natural aquifers and has been studied extensively in hydrogeology (e.g., Chang et al., 2016; Feng et al. 2020; Hsieh et al., 2014; Li et al. 2020; Li et al. 2021; Liang et al. 2019; Sedghi et al., 2021). The riverbank often has two-layers structure which is composed of non-cohesive and cohesive materials (Thorne and Tovey 1981). Heterogeneity in riverbank sediments not only controls water exchange by deflecting flow downward into the sediment or upward into the channel (Ward et al. 2011), but it also alters groundwater paths, fluxes, and residence times in the riparian zone (Earon et al. 2020; Gomez-Velez et al. 2014; Pryshlak et al. 2015; Sawyer et al. 2009). Sawyer and Cardenas (2009) conducted numerical simulations of hyporheic flow and solute transport through immobile bed forms composed of heterogeneous sediments. Their findings showed that the sediment heterogeneity created longer hyporheic mixing paths than the case with homogeneous sediments. Liang and Zhang (2013) presented an analytical solution for the water table and lateral discharge in a heterogeneous unconfined aquifer with a time-dependent source and fluctuating river stage. The heterogeneity that they considered consists of a number of sections of different hydraulic conductivity values. More recently, Su et al. (2020) evaluated the scale issues inherent in concentration, mixing, heterogeneity, and modelling approaches in hyporheic flow based on a numerical model and Monte Carlo simulations. Their results revealed that flux variance in the streambed is an appropriate metric for assessing the magnitude of hyporheic mixing at all scales.

Previous work evaluating the heterogeneity of aquifers in analytical models is summarized in Table 1. To the best of our knowledge, a 2-D analytical model describing groundwater flow in the riparian zone (or hyporheic zone) with a two-layer structure has not been reported. Therefore, this study aims to fill this knowledge gap by presenting a semi-analytical solution for this 2-D model. In the semi-analytical model, groundwater flow in the two layers is coupled with the continuity of the hydraulic head and water fluxes across the interface. We anticipate that the proposed semi-analytical model could be used to investigate changes of the hydraulic head and lateral discharge caused by a recharge or flood event in a layered aquifer system. The paper is organized as follows: the mathematical model and its solution are presented in section 2 and section 3, respectively. The comparison of the solution with a high-resolution numerical model built with COMSOL is given in section 4. The results and discussion are presented in section 5 and application of the solution to field data is described in section 6. Section 7 presents the summary and conclusions from this work.

2. Conceptual and Mathematical Models

A schematic diagram of groundwater flow along a transect of the riparian zone in a two-layer unconfined aquifer is displayed in Fig. 1. The layered aquifer is laterally bounded by a watershed divide and a river that fully penetrates the aquifer (Fig. 1a), which is conceptualized in two dimensions (Fig. 1b). In Fig. 1b, the x-axis is along the groundwater flow direction toward the divide, and the z-axis is vertically upward. The top of the aquifer is the water table, which receives time-dependent recharge from rainfall events. The bottom of the aquifer is horizontal and impermeable. The upper and lower layers have a uniform initial thickness of B_1 [L] and B_2 [L], respectively. The upper and lower layers are both homogeneous, but their hydraulic conductivities are different. The governing equation for groundwater flow in the aquifer is given as follows:

$$S_{s1}\frac{\partial h_1}{\partial t} = K_{x1}\frac{\partial^2 h_1}{\partial x^2} + K_{z1}\frac{\partial^2 h_1}{\partial z^2},\ 0 \le z \le \xi,\ 0 \le x \le L \tag{1a}$$

$$S_{s2}\frac{\partial h_2}{\partial t} = K_{x2}\frac{\partial^2 h_2}{\partial x^2} + K_{z2}\frac{\partial^2 h_2}{\partial z^2},\ -B_2 \le z \le 0,\ 0 \le x \le L \tag{1b}$$

The initial head is defined as a uniform value:

$$h_1(x,z,t) = h_2(x,z,t) = H_0,\ t = 0 \tag{2a}$$

and the boundary conditions are defined as:

$$h_1(x,z,t) = h_2(x,z,t) = H_b(t),\ x = 0 \tag{2b}$$

$$\frac{\partial h_1}{\partial x}(x,z,t) = \frac{\partial h_2}{\partial x}(x,z,t) = 0,\ x = L \tag{2c}$$

$$\frac{\partial h_2}{\partial z}(x,z,t) = 0,\ z = -B_2 \tag{2d}$$

where subscripts 1 and 2 represent the upper and lower layer, respectively; S_s is the specific storage [L^{-1}]; h is the hydraulic head [L]; K_x and K_z are hydraulic conductivity in x-direction (horizontal) and z-direction (vertical), respectively; ξ is the instantaneous location of the moving water table; H_0 is the initial head, which is the same as water table [L]; and $H_b(t)$ is the fluctuating river stage [L].

Eqs. (1a) and (1b) are coupled by the interface conditions representing the continuity of the hydraulic head and vertical fluxes, respectively (Liang et al., 2017a; Liang et al., 2017b):

$$h_1(x, z=0, t) = h_2(x, z=0, t),\ \ z = 0 \tag{3a}$$

$$K_{z1}\frac{\partial h_1}{\partial z}(x, z, t) = K_{z2}\frac{\partial h_2}{\partial z}(x, z, t),\ \ z = 0 \tag{3b}$$

The upper boundary of the unconfined aquifer with a recharge term is a free surface (moving water table) that can be described by the following equation (Bear,1979, P.99):

$$[K_{z1} + W(t)]\frac{\partial h_1}{\partial z} = -S_y\frac{\partial h_1}{\partial t} + W(t) + K_{x1}\left(\frac{\partial h_1}{\partial x}\right)^2 + K_{z1}\left(\frac{\partial h_1}{\partial z}\right)^2,\ z = \xi \tag{4a}$$

where S_y is the specific yield [-]; and $W(t)$ is the time-dependent recharge rate [LT^{-1}]. The coupled equations (1)- (3) are difficult to solve analytically because of the nonlinear nature of upper boundary condition (4a) and the unknown location of the moving water table ξ. To resolve this issue, Eq. (4a) is linearized by using the perturbation technique (Dagan, 1964), which is widely adopted to simulate water flow in unconfined aquifers (e.g., Malama et al., 2011; Neuman, 1972; Zhan and Zlotnik, 2002). First, the water table is imposed on a fixed position ($z = B_1$) by assuming that the magnitude of water table fluctuation is much less than the aquifer thickness. Second, the two quadratic terms are ignored because they are much smaller than the other terms of Eq. (4a). Finally, the recharge term on the left side of Eq. (4a) is also ignored because the aquifer recharge rate W is usually orders of magnitude smaller than the hydraulic conductivity K_{z1}. Based on the above assumptions, the water table boundary can be simplified to the linearized form:

$$K_{z1}\frac{\partial h_1}{\partial z} = -S_y\frac{\partial h_1}{\partial t} + W(t),\ z = B_1 \quad \text{(4b)}$$

To test the validity of the linearized boundary condition (4b), we conduct a numerical experiment to compare the nonlinear (4a) and linearized boundary conditions (4b). Specifically, the coupled equations (1)- (3) with the boundary conditions (4a) and (4b) are solved numerically, respectively. Then the hydraulic heads predicted by the model with the nonlinear boundary (4a) is compared to that of the model with the linearized boundary (4b). It should be noted that the nonlinear boundary in the numerical model is fixed at $z = B_1$ rather than the moving water table, which requires the magnitude of water table fluctuation to be much less than the aquifer thickness. The details are presented in the supporting information (S4). The results indicate that the error caused by ignoring the quadratic terms and the recharge term on the left side of Eq. (4a) is very small when the recharge rate is less than one tenth of the vertically hydraulic conductivity, which is widespread in the real world. It implies that the linearized boundary (4b) is an appropriate approximation to the moving water table boundary.

3. Solutions

3.1 Solutions for hydraulic head

The governing equation (1) are solved by the Laplace and the Fourier sine transforms, and the details of the derivation are presented in the supporting information (S1). The Laplace domain solutions of Eqs. (1a) and (1b) with the initial condition (2a) and boundary conditions (2)- (4) can be respectively written as:

$$\bar{h}_{1D}(x_D, z_D) = \bar{h}_{bD} + \sum_{n=0}^{\infty}[C_{1a}\,exp(-\Omega_{1n}z_D) + C_{1b}\,exp(\Omega_{1n}z_D) - \lambda_1]\sqrt{2}\sin(\omega_n x_D) \quad \text{(5a)}$$

$$\bar{h}_{2D}(x_D, z_D) = \bar{h}_{bD} + \sum_{n=0}^{\infty}[C_{2a}\, exp(-\Omega_{2n} z_D) + C_{2b}\, exp(\Omega_{2n} z_D) - \lambda_2]\sqrt{2}\sin(\omega_n x_D) \qquad (5b)$$

where the subscript 'D' denotes the dimensionless terms hereinafter; the overbar denotes a variable in the Laplace domain; the definition of all dimensionless variables is summarized in Table 2 and the supporting information (S1); and the definitions of variables $C_{1a}, C_{1b}, C_{2a}, C_{2b}, \Omega_{1n}, \Omega_{2n}, \lambda_1, \lambda_2,$ and ω_n are presented in the supporting information (S3).

3.2 Solutions for lateral discharge

On the basis of Darcy's Law, the lateral discharge of groundwater per unit width along the river channel (at $x = 0$) can be expressed as the sum of lateral discharges for two layers as follows:

$$Q(t) = Q_1(t) + Q_2(t) = -\int_0^{B_1} K_{x1} \frac{\partial h_1}{\partial x}|_{x=0} dz - \int_{-B_2}^{0} K_{x2} \frac{\partial h_2}{\partial x}|_{x=0} dz \qquad (6)$$

where $Q_1(t)$ and $Q_2(t)$ are the lateral discharge of layer 1 and layer 2, respectively [$L^2 T^{-1}$]. Eq. (6) can be transformed to its dimensionless form:

$$Q_D(t_D) = Q_{1D}(t_D) + Q_{2D}(t_D) = -\frac{1}{\sqrt{R_K}}\int_0^{B_{1D}} \frac{\partial h_{1D}}{\partial x_D}|_{x_D=0} dz_D - \sqrt{R_K}\int_{-B_{2D}}^{0} \frac{\partial h_{2D}}{\partial x_D}|_{x_D=0} dz_D (7)$$

where $R_K = K_{x2}/K_{x1}$; and the other definitions of dimensionless parameters can be found in Table 2. Conducting Laplace transform on Eq. (7) yields the following:

$$\bar{Q}_D = \bar{Q}_{1D} + \bar{Q}_{2D} = -\frac{1}{\sqrt{R_K}}\int_0^{B_{1D}} \frac{\partial \bar{h}_{1D}}{\partial x_D}|_{x_D=0} dz_D - \sqrt{R_K}\int_{-B_{2D}}^{0} \frac{\partial \bar{h}_{2D}}{\partial x_D}|_{x_D=0} dz_D \qquad (8)$$

Substituting Eqs. (5a) and (5b) into Eq. (8) leads to:

$$\bar{Q}_{1D} = -\sqrt{\frac{2}{R_K}}\sum_{n=0}^{\infty} \omega_n \left[\frac{C_{1a}(1-\exp(-\Omega_{1n}B_{1D})) + C_{1b}(\exp(\Omega_{1n}B_{1D})-1)}{\Omega_{1n}} - \lambda_1 B_{1D}\right] \qquad (9a)$$

$$\bar{Q}_{2D} = -\sqrt{2R_K}\sum_{n=0}^{\infty} \omega_n \left[\frac{C_{2a}(\exp(\Omega_{2n}B_{2D})-1) + C_{2b}(1-\exp(-B_{2D}\Omega_{2n}))}{\Omega_{2n}} - \lambda_2 B_{2D}\right] \qquad (9b)$$

$$\bar{Q}_D = \bar{Q}_{1D} + \bar{Q}_{2D} = -\sqrt{\frac{2}{R_K}}\sum_{n=0}^{\infty}\omega_n\left[\frac{C_{1a}(1-\exp(-\Omega_{1\mathrm{n}}B_{1D})) + C_{1b}(\exp(\Omega_{1\mathrm{n}}B_{1D})-1)}{\Omega_{1\mathrm{n}}} - \lambda_1 B_{1D}\right]$$

$$-\sqrt{2R_K}\sum_{n=0}^{\infty}\omega_n\left[\frac{C_{2a}(\exp(\Omega_{2\mathrm{n}}B_{2D})-1) + C_{2b}(1-\exp(-B_{2D}\Omega_{2\mathrm{n}}))}{\Omega_{2\mathrm{n}}} - \lambda_2 B_{2D}\right] \tag{9c}$$

3.3 Solutions for fluxes between two layers

Water exchange occurs between the two layers of the aquifer induced by fluctuating river stage and by recharge events. Darcy's velocity across the interface of the two layers is:

$$q_E(x,t) = -K_{z1}\frac{\partial h_1}{\partial z}|_{z=0} \tag{10}$$

Based on Eq. (5a), the dimensionless Darcy's velocity across the interface can be written as:

$$\bar{q}_{ED}(x_D) = \sqrt{2}\frac{K_{1\mathrm{D}}}{\sqrt{R_K}}\sum_{n=0}^{\infty}\Omega_{1n}(C_{1b}-C_{1a})\sin(\omega_n x_D) \tag{11}$$

Given Eq. (11), the dimensionless exchange fluxes along the interface of two layers can be obtained by:

$$\bar{Q}_{ED} = \int_0^1 \bar{q}_{ED}(x_D)dx_D = \sqrt{2}\frac{K_{1\mathrm{D}}}{\sqrt{R_K}}\sum_{n=0}^{\infty}(C_{1b}-C_{1a})\frac{\Omega_{1n}}{\omega_n} \tag{12}$$

Both solutions of head and discharge presented above involve the time-varying river stage $H_b(t)$ and recharge rate $W(t)$. Both river stage and recharge should be specified if one aims to evaluate the head and discharge. In this study, the river stage is presented by a piecewise-linear function with time, and the recharge rate is presented by a piecewise-constant function with time. Therefore, $H_b(t)$ and $W(t)$ can be written in the following forms:

$$H_b(t) = \frac{H_{bi}-H_{bi-1}}{t_i - t_{i-1}}(t - t_{i-1}) + H_{bi-1}, \quad t_{i-1} \le t < t_i \tag{13a}$$

$$W(t) = W_j, \quad t_{i-1} \le t < t_i \tag{13b}$$

where H_{bi} is the observed river stage at time t_i; and W_j is a constant for the time interval $t_{i-1} \le t < t_i$ with $t_0 = 0$. The piecewise-linear approximation is the most practical approach for treating the actual river stage because it permits approximation of any river hydrograph with desired accuracy if small time increments are used (Liang et al., 2020). Taking dimensionless and Laplace transform on Eqs. (13a) and (13b) yields:

$$\overline{H}_{bD} = \sum_{i=1}^{\infty} e^{-pt_{Di-1}} \frac{\alpha_i + pH_{Di-1}}{p^2} - e^{-pt_{Di}} \left[\frac{\alpha_i(1+pt_{Di})}{p^2} + \frac{(H_{Di-1}-\alpha_i t_{Di-1})}{p}\right] \quad (14a)$$

$$\overline{W}_D = \sum_{i=1}^{\infty} \frac{W_{Di}}{p} [\exp(-pt_{Di-1}) - \exp(-pt_{Di})] \quad (14b)$$

where p is the Laplace transform parameter; α_i is the variation rate of the hydraulic head during t_{Di} to t_{Di-1}; and the definitions of dimensionless variables H_{bD} and W_D are presented in Table 1.

Eqs. (5), (9), (11), and (12) are the Laplace domain solutions. Due to the complicated mathematical expressions, it is challenging to obtain closed-form solutions by inverse Laplace transforms analytically. There are, however, several numerical inverse Laplace methods that fix this problem, such as the Zakian method (Zakian, 1969), Fourier series method (Dubner and Abate, 1968), Stehfest method (Stehfest, 1970), Crump technique (Crump, 1976), Talbot algorithm (Talbot, 1979), and de Hoog algorithm (de Hoog et al., 1982). We choose the de Hoog algorithm to invert the Laplace solutions into the time domain because a solution involving the piecewise functions Eqs. (13a) and (13b) commonly requires complex versions of the numerical inverse Laplace method (Liang et al., 2017).

4. Comparison with Numerical Solutions

To test the validity of the semi-analytical solutions Eqs. (5) and (9), we compared them with the numerical solutions of the dimensionless governing Eq. (S1). The dimensionless parameter values of the model are: $K_{1D} = 1, K_{2D} = 1, R_K = 0.1, B_{1D} = 0.04, B_{2D} = 0.04,$ and $S_{yD} = 0.8$. Synthetic numerical simulations are carried out for two scenarios: (1) groundwater flow induced by two rainfall recharge events which occur at $0.5 \leq t_D < 1.0$ with a constant rate of $W_D = 0.2$, and $3.0 \leq t_D < 3.5$ with a constant rate of $W_D = 0.8$ (Fig. 2a), and the river stage is constant or $H_{bD} = 1$; and (2) groundwater flow induced by a flood event, in which the dimensionless river hydrograph is described with a diffusive-type flood wave (Fig. 2b), and no recharge or $W_D = 0$.

The dimensionless governing Eqs. (S1) are numerically solved using COMSOL Multiphysics (COMSOL Inc., Burlington, MA, U.S.A.), a Galerkin finite-element software package that includes a partial differential equation (PDE) solver for modelling the type of governing equations of this study. Triangulations are used for the elements of the 2-D cross-section domain. To ensure sufficient accuracy of the simulation, the elements near the water table, the interface between two layers, and the river are refined with the minimum mesh-size of 0.002 and the maximum mesh-size of 0.01, which includes 28860 triangular elements and 14799 nodes. The time step Δt_D is 0.0025 for the two scenarios.

Figs. 2c and 2d show the responses of the hydraulic heads in the upper layer and the lower layer to the recharge and the flood events, respectively. Figs. 2e and 2f also present the lateral discharge induced by the recharge and the flood events, respectively. These figures indicate that the analytical solutions (solid curves) for both hydraulic head and discharge well agree with those of numerical solutions (circle symbols) over the entire simulation period. Through the above comparison, the analytical solutions of this study appear to be acceptable to predict the hydraulic heads and the discharges for the model.

5. Results and Discussion

5.1 Effects of layered heterogeneity on hydraulic heads

In this study, the layered heterogeneity is mainly represented by a dimensionless parameter $R_K = K_{x2}/K_{x1}$ that quantifies the contrast in hydraulic properties of the two layers. We first investigate how the layered heterogeneity impacts the responses of hydraulic heads to the time-varying recharge and the fluctuating river stage. To clearly demonstrate the impacts of R_K, we assume that the aquifer is isotropic, and the specific storage of two layers are equal. The other parameters of the aquifer are as follows: $K_{1D} = 1, K_{2D} = 1, R_S = 1, B_{1D} = 0.04, B_{2D} = 0.04,$ and $S_{yD} = 0.8$.

Fig. 3 displays the responses of the hydraulic heads to a recharge event ($W_D = 0.25$ during $0.5 \leq t_D < 1.0$) and a flood wave for different values of R_K (0.01, 1.0, and 100). Figs. 3b and 3c show that R_K has a significant impact on the responses of hydraulic heads to the recharge event. For the large R_K (=100), the hydraulic head in the upper layer (blue solid curve) is markedly larger than that of the lower layer (blue triangle symbol). For the small R_K (=0.01), the hydraulic head in the upper layer (red solid curve) is close to that of the lower layer (red triangle symbol). Furthermore, for the homogeneous case ($R_K = 1$), the hydraulic head in the upper layer (cyan solid curve) is the same as that of the lower layer (cyan triangle symbol). These observations indicate that the aquifer has a significantly downward hydraulic gradient induced by the recharge when the upper layer has a smaller permeability. In contrast, for the case of the larger permeability in the upper layer, the aquifer has no obvious vertical hydraulic gradient, which is similar to the homogeneous case. These observations imply that the heterogeneous hydraulic conductivity regulates the groundwater flow path. The upper layer with the low permeability hinders groundwater lateral discharging into the river in the upper layer and forces water to flow downward into the highly permeable layer. In contrast, when the upper layer has a high permeability, it provides a fast flow path for the lateral discharge in the upper layer and prevents water from flowing downward into the lower layer.

Fig. 3e presents the response of the hydraulic heads to the flood event. Similar to the case of the recharge event, there is little difference in hydraulic heads between the upper and lower layers for the homogenous case ($R_K = 1$) and the case in which the upper layer has a higher permeability ($R_K = 0.01$). For the case in which the upper layer has a lower permeability ($R_K = 100$), however, the hydraulic head in the upper layer (blue solid curve) is significantly lower than that of the lower layer (blue triangle symbol) in the early time ($t_D < 0.3$), and the hydraulic head in the upper layer becomes higher in the later time. The hydraulic head profile (Fig. 3f) further illustrates that for the case of $R_K = 100$ the aquifer has a markedly upward hydraulic gradient at $t_D = 0.1$ (the rise phase of heads), and it has a markedly downward hydraulic gradient at $t_D = 0.4$ (the decline phase of heads). For the cases of $R_K = 0.01$ and 1, the vertical hydraulic gradients are small, which is in accordance with the observations in Fig. 3d. The diverse hydraulic gradients reflect the impacts of heterogeneity on the water flow path. When the upper layer has a lower permeability, most of the river water initially infiltrates into the lower layer during the flood period and then flows upward into the upper layer. The flow pattern changes in reverse during the recession period. When the upper layer has a higher permeability, the vertical flow in the aquifer is not obvious, which will be further illustrated later.

To clearly illustrate the effects of the layered heterogeneity, the vertical profiles of the hydraulic heads for the different R_K (0.01, 1, and 100) induced by the recharge event and the flood event based on our semi-analytical solution are presented in Figs. 4 and 5, respectively. The other parameter values are the same as those in Fig. 3. Fig. 4 indicates that there is no significant vertical hydraulic gradient when $R_K \leq 1$, while the downward hydraulic gradient is evident when $R_K > 1$. This means that the heterogeneity does not necessarily cause the discrepancies in hydraulic heads between the two layers; the differences in hydraulic heads between the two layers only occur when the upper layer is less permeable than the lower layer. In the other case, the difference in hydraulic heads is miniscule. In addition, Fig. 4 also shows that the hydraulic heads of both cases of $R_K = 0.01$ and $R_K = 100$ are generally larger than that of the case of $R_K = 1$ for the different times. This implies that the heterogeneity leads to faster recession processes for the aquifer and results in the lower hydraulic heads. For the flood event, the impacts of the heterogeneity are similar to the case of the recharge event. The hydraulic heads between the two layers differ only when the upper layer is less permeable than the lower layer. However, the difference with the case of the recharge event is that the aquifer has an upward hydraulic gradient during the rising phase of the hydraulic heads, and a downward hydraulic gradient during the declining phase. This means that there is a significant water interaction between the two layers induced by the flood event when the hydraulic conductivity of the upper layer is lower than that of the lower layer.

5.2 Effects of layered heterogeneity on lateral discharge

In this section, we investigate the effects of layered heterogeneity on the recession processes induced by a recharge event and the river-aquifer exchange induced by a flood event. Fig. 6b displays the discharge (baseflow) recession induced by a recharge event (Fig. 6a) for the different R_K (0.01, 1, and 100). The other parameters are the same as those in Fig. 3. Fig. 6b shows that the discharge has a larger peak value and a faster recession process when R_K is small. For the large R_K (=100), the discharge has a smaller peak value and a slower recession process. This means that when the upper layer has a high permeability, water from the recharge event will be quickly discharged into the river. When the upper layer has a low permeability, most of the water from the recharge event will infiltrate into the lower layer. Meanwhile, for the homogeneous case ($R_K = 1$), the discharge has the smallest peak value and the slowest recession process. This is because we use the geometric mean of the hydraulic conductivity in the heterogeneous case to describe the hydraulic conductivity in the homogeneous case, which would be controlled by the minimum value.

Fig. 6d shows the response of river-aquifer exchanges to a flood event (Fig. 6c) for different R_K (0.01, 1, and 100). The discharge is negative in the early phase and positive in the later phase, which means that the aquifer receives water from the river at the beginning and then releases it to the river. For the small R_K (=0.01), however, the interaction between river and aquifer is much greater and more water migrates into the aquifer and then back into the river. For the large R_K (=100), the interaction is less than that in the small R_K case, and the arrival time of peak inflow and peak discharge lags compared with that in the small R_K case. This indicates that when the upper layer has a high permeability, the exchange between aquifer and river is more rapid. When the lower layer has a high permeability, there is a marked vertical hydraulic gradient (which can be found in Fig. 5). In the early phase, the vertical hydraulic gradient causes some water in the lower layer to migrate to the upper layer, which reduces peak inflow and delays the arrival time of peak inflow. In the later phase, the hydraulic gradient and exchange flow reverse and water from the upper layer migrates to the lower layer reduces peak discharge and delays the arrival time of peak discharge. For the homogeneous case ($R_K = 1$), the discharge has the smallest peak inflow and peak discharge. The reason for this is the same as that for the recharge event.

Equivalent hydraulic conductivity is often employed to simplify heterogeneity. For groundwater flow parallel to aquifer layers, the equivalent hydraulic conductivity is equal to the arithmetic mean of all individual hydraulic conductivities of the layers (Eq. 15a). For groundwater flow perpendicular to aquifer layers, the equivalent hydraulic conductivity is equal to the harmonic mean of all individual hydraulic conductivities of the layers (Eq. 15b).

$$K_p = \frac{\sum_1^n K_i B_i}{\sum_1^n B_i} \tag{15a}$$

$$K_v = \frac{\sum_1^n B_i}{\sum_1^n \frac{B_i}{K_i}} \tag{15b}$$

where K_i is the hydraulic conductivity of layer i; and B_i is the thickness of layer i. However, the equivalent method is derived based on a steady flow. In order to verify the applicability of the equivalent formula in the riparian zone, we employ the equivalent hydraulic conductivity on transient lateral discharge.

It should be noted that the result has to be discussed with dimension, as the hydraulic conductivity influences the dimensionless form of time. In this part, the hydraulic conductivities are $1(\ m/d)$ and $10(\ m/d)$ for the upper layer and the lower layer, respectively. Therefore, the arithmetic mean would be $5.5(\ m/d)$ and the harmonic mean would be $1.8(\ m/d)$. The other parameters of the aquifer are as follows: $S_{s1} = S_{s2} = 0.001(m^{-1})$, $S_y = 0.2$, $B_1 = B_2 = 10(m)$, $L = 250(m)$. These parameters would be the same as those in Fig. 2 if we transform them into dimensionless form.

Fig. 7a presents the responses of lateral discharge to a recharge event for arithmetic mean, harmonic mean, and the heterogeneous aquifer. When the arithmetic mean (red curve) is employed, the lateral discharge is remarkably smaller than that in the heterogeneous case. Meanwhile, in the recession process, the difference between them decreases. When the harmonic mean (blue curve) is employed, the lateral discharge is similar to that in the heterogenous case at the beginning, but the lateral discharge based on harmonic mean decreases more slowly than that in the heterogenous case after 60 d. Fig. 7b shows the responses to a flood event. When the arithmetic mean (red curve) is employed, the interaction between river and aquifer is much less, and the arrival time of peak value is earlier, than that in heterogeneous case. When the harmonic mean (blue curve) is used, the interaction would be overestimated, and the arrival time of peak value for the harmonic mean is slightly earlier than that in the heterogeneous case. These observations indicate that, for both the recharge event and flood event, the harmonic mean would overestimate the discharge and the arithmetic mean would underestimate it. The reason for this is that the arithmetic mean depends on the large hydraulic conductivity and would overestimate the overall hydraulic conductivity. In comparison, the harmonic mean depends on the small hydraulic conductivity and would underestimate the overall hydraulic conductivity.

5.3 Exchange fluxes between two layers

The dimensionless exchange flux across the interface between the two layers q_D is the direct reflection of the impacts of the contrast in properties between the two considered layers on groundwater flow. To gain insight into the pattern of the exchange flux, Fig. 8 displays the spatial distribution of q_D along the interface at different times for a recharge event (Fig. 8a) and flood event (Fig. 8b). The parameters used in Fig. 8 are the same as those in Fig. 2. For a recharge event (Fig. 8a), all q_D values are negative, which means that the groundwater in the upper layer migrates into the lower layer. There is a peak of q_D close to the left boundary in the early phase. This peak value increases over time, and the location of the peak value moves toward the right as time progresses, as well. When the recharge process ends ($t_D = 1$), the flux from the upper layer decreases. However, some groundwater in the upper layer still flows across the interface into the lower layer.

For a flood event (Fig. 8b), all q_D values are positive in the early phase, which means that water in the lower layer migrates into the upper layer. In addition, q_D varies with x_D, and the peak of q_D is close to the left boundary. This peak value increases by $t_D = 0.1$ before decreasing, and the location of the peak value moves toward the right as time progresses. In the flood recession process, the flux at the left region gently becomes negative, which means that the water in the upper zone migrates into the lower layer in this region. However, some water in the lower layer still flows across the interface into the upper layer at the right regions. As time passes, q_D gradually becomes negative at more locations of the interface, which indicates that the water flowing from the upper layer into the lower layer gradually dominates the exchange flux between the two regions.

To investigate the impacts of the distinction in properties between the two considered layers on the total exchange flux between the two regions, the response of dimensionless total exchange flux over the interface ($Q_{exD}(t_D)$) to a recharge event and a flood event for different R_K(0.01, 1, and 100) are presented in Fig. 9. Q_{exD} is evaluated using the integration of q_{exD} over the interface, i.e., $Q_{exD}(t_D) = \int_0^1 q_{exD} dx_D$. The other parameters used in Fig. 9 are the same as those in Fig. 3. For the recharge event (Fig. 9a), exchange flow from the upper layer to the lower layer increases as the recharge event occurs, and then decreases to zero gradually after the recharge. It can also be noticed that for a larger R_K, there is more water migrating into the lower layer. These observations are consistent with the conclusions reached above, namely that an upper layer with the low-permeability forces water to flow downward into the highly permeable layer. When the upper layer has a high permeability, it would provide a fast flow path for the lateral discharge, and the lower layer would function as an aquitard. For the flood event (Fig. 9b), the total exchange between layers is maximized when R_K increases. For a small R_K, the amount of water being exchanged between layers is small. For a large R_K, the upper layer releases more water to the lower layer in the early phase and then the water moves back, there is a slight downward vertical exchange. For the homogeneous case, the mechanism of exchange flow is similar to that for a large R_K with a smaller peak and bottom. These findings suggest that when the upper layer has a high permeability, the vertical hydraulic gradient becomes smaller and the upper layer with the low-permeability would result in a larger vertical hydraulic gradient, although the direction is opposite.

6. Application to Field Data

The present solution is applied to observed hydraulic heads in a riparian zone on White Clay Creek within the Christina River Basin Critical Zone Observatory in Southeastern Pennsylvania (Sawyer et al., 2014). The riparian zone has a two-layer structure. The upper layer includes organic-rich silt and silty clay, whose hydraulic conductivity ranges from 0.47×10^{-6} m/s to 4.7×10^{-6} m/s. The lower layer is silty gravel, whose hydraulic conductivity ranges from 0.59×10^{-6} m/s to 59×10^{-6} m/s. Five observation wells (referred to as well 110, 119, 120, 121, and 122) are installed in the west bank. The details of the field are provided in Sawyer et al. (2014).

The measured precipitation and river stage are presented in Fig. 10a. The analytical model is applied to simulate the response of the hydraulic head to the storm. The change of the hydraulic head (ΔH) relative to its initial value is employed to fit the present model. The aquifer recharge is difficult to estimate directly but it is usually proportional to the precipitation, which is helpful in estimating recharge. Here we assume that the recharge is proportional linearly to the precipitation with an unknown ratio R_{pi}. Thus, the recharge can be obtained by estimating the ratio of the recharge and precipitation R_{pi}. The aquifer parameters are estimated by minimizing the sum of the squared differences between simulated and observed heads. The estimated parameters are: $K_1 = 0.1m/d, K_2 = 2m/d, S_y = 0.021, S_{s1} = S_{s2} = 1 \times 10^{-5}\ 1/m, B_1 = 1.0m, B_2 = 6.0m, L = 60m$, and $R_{pi} = 0.2$. The initial water table is equal to the river stage (H=101.4 m), and the interface between the two layers is located at 100.9 m. It should be noted that the thicknesses of the upper and lower layers are presumed by combining the distribution of soils and comparing of the analytical solutions with the observation data.

Fig. 10b shows that the present solution agrees with the observed hydraulic heads of four wells, while it performs poorly for well 122. The reason for this is that the observed values in well 122 might be affected by the unsaturated zone, which is not considered in the present solution. Furthermore, the change of hydraulic head in well 122 is the highest, which implies that the recharge event has a greater impact on the hydraulic head than does the flood event. This is because the upper layer with the lower-permeability has a higher hydraulic head in the recharge event and a lower hydraulic head in the flood event, as displayed in Figs. 4 and 5, respectively. Furthermore, a clear tail phenomenon exists in each well and, when the well is further away from the river, this phenomenon is more obvious. This is attributable to the fact that a well that is far from the river needs more time to discharge the water received from precipitation.

To further investigate the effect of a two-layer structure on this case for the recharge event, precipitation, exchange flux, and discharge are shown in Fig. 11. Fig. 11a presents precipitation, total exchange flux between the two layers, and discharge from both layers against time. To make the difference between total exchange flow and discharge clearer, the absolute value of total exchange flow is presented in Fig. 11a. It can be seen in Fig. 11a that the peak of precipitation and total exchange flux between the two layers appear in chronological order, and total exchange flux between the two layers is almost same as discharge from the lower layer. The time difference between precipitation and total exchange flux is 0.6 d. The discharge from the upper layer is minimal compared with that from the lower layer. These phenomena reflect the path of groundwater flow in White Clay Creek. With the recharge by precipitation, most of the groundwater would flow into the lower layer and discharge to the river. Four specific times are selected to examine the exchange flux, i.e., before the storm (t = 0.5 d), during the storm (t = 1.22 d), at the peak of total exchange flux (t = 1.75 d) and after the storm (t = 3.75 d), as shown in Fig. 11b. Before the storm, the exchange flux is almost zero everywhere. During the storm (t = 1.22 d), the location of the peak values of exchange flux are near the left boundary. Moreover, the exchange flux is positive at the left region and negative at the other regions. This means that the water in the lower layer migrates into the upper layer at the left region due to the stage of the rising river; at the other regions, the recharge event and the upper layer with lower-permeability cause a downward vertical exchange flow. When the total exchange flow reaches its maximum (t = 1.75 d), the flux at all regions is negative, and there is a trough near the left boundary. This means that the water in the upper layer migrates into the lower layer, and the decreasing stage of the river would result in a higher exchange flux near the left boundary. After the storm (t = 3.75 d), the flux at all regions is both negative and small. This indicates that the upper layer with the low-permeability exerts a damping effect on downward exchange flow, and the small and longstanding discharge to the lower layer would lead to the tailing phenomenon observed in Fig. 11a.

Results from the case study shown above clearly show that the 2-D semi-analytical model is capable of capturing the dynamic interactions of a two-layered aquifer in response to recharge and flooding. Here we comment on the utility of the approach more broadly and potential implications. Two-layered aquifer systems are commonly found in floodplains and riparian zones and in many areas, the upper fine-textured layer is intensely cropped (e.g., Kalkhoff et al., 1992; Wang and Squillace, 1994; Devito et al., 2000). Applications of nitrogen fertilizer (Kalkhoff et al., 1992) and herbicides (Squillace et al., 1994) applied to the upper layer are potentially mobilized to the more permeable lower layer during recharge and flood events. Similarly, two-layered systems occurring in riparian zones will have implications for implementing conservation practices designed to remediate subsurface contamination such as riparian buffers (Mayer et al., 2007) and saturated buffers (Jaynes and Isenhart, 2014). These riparian buffer practices are most effective when groundwater flow high in nitrogen interacts with the organic rich sediments. Hence, two-layered alluvial aquifers and riparian zones found along many rivers and streams may be severely compromised by variable hydraulic gradients imposed from periodic recharge and flood events and more work is needed to apply the 2-D semi-analytical model to these conditions.

Finally, there are a number of limitations that should be addressed for better application of the semi-analytical solution of this study. First, the present solution does not consider the impacts of the semipervious riverbed. The hydraulic conductivity of riverbed is usually lower than that of the aquifer and it will dampen surface-groundwater exchanges, depending on the riverbed hydraulic conductance (Huang et al., 2014; Sun & Zhan, 2007). The impacts of the semipervious riverbed can be considered by replacing the Dirichlet boundary condition on the river with a Robin (or third-type) boundary condition. Second, the heterogeneous aquifer we considered is caused by the layered structure of the riparian zone. The heterogeneity of the realistic riparian zone, however, is more complicated. For example, the macropores will provide preferential vertical flow paths. the lens and plant roots in riparian zone will obstruct groundwater flow. These all enhance the heterogeneity of the aquifer and limit application of the present solution. Third, the linearized water table boundary (4b) requires that the magnitude of water table fluctuation is much less than the aquifer thickness. However, it is difficult to address exactly how small is “much less”. This question may be addressed by comparison the present model with a numerical model that considers free moving water table. However, such model will involves complicated moving-mesh treating and iterative solving on unknown water table, which could be the future work.

7. Conclusion

In this study, groundwater responses to recharge and flood in the riparian zone of a two-layer aquifer were investigated and a 2-D semi-analytical model describing groundwater flow in the layered heterogeneous medium was developed. Groundwater flow in the two layers is governed by the 2-D transient groundwater flow equation and is coupled by the continuity of the hydraulic head and groundwater fluxes across the interface between the two layers. The semi-analytical solutions for the hydraulic heads in the two layers are derived and compared with a finite-element solution using COMSOL Multiphysics and applied to field data in White Clay Creek. The following conclusions can be drawn from this study:

(1) The two-layer structure has a significant effect on the responses of groundwater flow to hydrological events. For recharge events when the upper layer is less permeable, lateral discharge to the river in this layer is impeded and more groundwater flows downward into

the more permeable lower layer. In contrast, when the upper layer is more permeable, more groundwater flows laterally into the river and less downward into the less permeable lower layer. For a flood event when the upper layer is less permeable, river water infiltrates mostly into the more permeable lower layer during the initial time of the flood period and then flows upward into the upper layer, creating a vertical flow from the more permeable lower layer to the less permeable upper layer. The direction of the vertical flow is reversed during the recession period. However, this phenomenon is not evident when the upper layer is more permeable than the lower layer.

(2) The comparison of discharge for the equivalent hydraulic conductivity and heterogeneous hydraulic conductivity shows that the equivalent hydraulic conductivity method can lead to large errors in discharge. For the recharge event, the peak discharge simulated with the harmonic mean of hydraulic conductivities is reasonable, but the discharge is overestimated during the recession process. The peak discharge simulated with the arithmetic mean of hydraulic conductivities would underestimate the peak discharge. For the flood event, the discharge simulated with the equivalent hydraulic conductivity method peaks earlier than it should be. Moreover, the interaction between river and aquifer simulated with the harmonic mean of hydraulic conductivities is overestimated, and that with the arithmetic mean of hydraulic conductivities is underestimated.

(3) The present solution is applied to model the observed hydraulic head and discharge in White Clay Creek within the Christina River Basin Critical Zone Observatory in Southeastern Pennsylvania, and the estimated values of the aquifer parameters are reasonable.

(4) Riparian flow controls the active chemical and biological processes in riparian zone, the present solution is a convenient calculation method for riparian flow in two-layer aquifer and

will provide a valuable and solid foundation to clarify chemical and biological reactions in riparian zones and alluvial aquifers.

Acknowledgement

This study was partially supported by research grants from the National Natural Science Foundation of China (No. 41977165, 42172275), the Natural Science Foundation of Shenzhen (JCYJ20190809142203633), and the State Environmental Protection Key Laboratory of Integrated Surface Water-Groundwater Pollution Control. We sincerely thank Associate Editor and reviewers for their constructive comments which help us improve the quality of the manuscript. Data used in preparing Fig. 10 of this manuscript are from Sawyer et al. (2014); no new data are used.

References

Boano, F., Camporeale, C., Revelli, R., Ridolfi, L., 2006. Sinuosity-driven hyporheic exchange in meandering rivers. Geophysical Research Letters, 33(18). DOI:10.1029/2006gl027630

Boano, F. et al., 2014. Hyporheic flow and transport processes: Mechanisms, models, and biogeochemical implications. Reviews of Geophysics, 52(4): 603-679. DOI:10.1002/2012rg000417

Butler, J.J., Zhan, X., Zlotnik, V.A., 2008. Pumping-induced drawdown and stream depletion in a leaky aquifer system - Reply. Ground Water, 46(4): 530-531. DOI:10.1111/j.1745-6584.2008.00422_2.x

Chang, C.M., Yeh, H.D., 2016. Investigation of flow and solute transport at the field scale through heterogeneous deformable porous media. Journal of Hydrology, 540: 142-147. DOI:10.1016/j.jhydrol.2016.05.060

Chang, Y.C., Yeh, H.D., Huang, Y.C., 2008. Determination of the parameter pattern and values for a one-dimensional multi-zone unconfined aquifer. Hydrogeology Journal, 16(2): 205-214. DOI:10.1007/s10040-007-0228-3

Chen, X., Chen, X.H., 2003. Stream water infiltration, bank storage, and storage zone changes due to stream-stage fluctuations. Journal of Hydrology, 280(1-4): 246-264. DOI:10.1016/s0022-1694(03)00232-4

Chuang, M.H., Huang, C.S., Li, G.H., Yeh, H.D., 2010. Groundwater fluctuations in heterogeneous coastal leaky aquifer systems. Hydrology and Earth System Sciences, 14(10): 1819-1826. DOI:10.5194/hess-14-1819-2010

Crump, K.S., 1976. Numerical inversion of laplace transforms using a fourier-series approximation. Journal of the Acm, 23(1): 89-96. DOI:10.1145/321921.321931

Curry, R.A., Gehrels, J., Noakes, D.L.G., Swainson, R., 1994. Effects of river flow fluctuations on groundwater discharge through brook trout, salvelinus-fontinalis, spawning and incubation habitats. Hydrobiologia, 277(2): 121-134. DOI:10.1007/bf00016759

Dagan, G., 1964. Second order linearized theory of free-surface flow in porous media. La Houille Blanche, 50(8): 901-910. DOI:10.1051/lhb/1964050

de Hoog, F.R., Knight, J.H., Stokes, A.N., 1982. An improved method for numerical inversion of laplace transforms. Siam Journal on Scientific and Statistical Computing, 3(3): 357-366. DOI:10.1137/0903022

de Mello, K., Valente, R.A., Randhir, T.O., dos Santos, A.C.A., Vettorazzi, C.A., 2018. Effects of land use and land cover on water quality of low-order streams in Southeastern Brazil: Watershed versus riparian zone. Catena, 167: 130-138. DOI:10.1016/j.catena.2018.04.027

Dubner, H., Abate, J., 1968. Numerical inversion of laplace transforms by relating them to finite fourier cosine transform. Journal of the Acm, 15(1): 115-+. DOI:10.1145/321439.321446

Earon, R., Riml, J., Wu, L.W., Olofsson, B., 2020. Insight into the influence of local streambed heterogeneity on hyporheic-zone flow characteristics. Hydrogeology Journal, 28(8): 2697-2712. DOI:10.1007/s10040-020-02244-5

Feng, Q.G., Liu, Z.W., Zhan, H.B., 2021. Semi-analytical solutions for transient flow to a partially penetrated well with variable discharge in a general three-layer aquifer system. Journal of Hydrology, 598. DOI:10.1016/j.jhydrol.2021.126329

Feng, Q.G., Luo, Y., Zhan, H.B., 2020. Three-dimensional response to a partially penetration well pumping in a general anisotropic three-layer aquifer system. Journal of Hydrology, 585. DOI:10.1016/j.jhydrol.2020.124850

Feng, Q.G., Yuan, X., Zhan, H.B., 2019. Flow to a partially penetrating well with variable discharge in an anisotropic two-layer aquifer system. Journal of Hydrology, 578. DOI:10.1016/j.jhydrol.2019.124027

Ferencz, S.B., Cardenas, M.B., Neilson, B.T., 2019. Analysis of the Effects of Dam Release Properties and Ambient Groundwater Flow on Surface Water-Groundwater Exchange Over a 100-km-Long Reach. Water Resources Research, 55(11): 8526-8546. DOI:10.1029/2019wr025210

Fritz, B.G., Arntzen, E.V., 2007. Effect of rapidly changing river stage on uranium flux through the hyporheic zone. Ground Water, 45(6): 753-760. DOI:10.1111/j.1745-6584.2007.00365.x

Gomez-Velez, J.D., Krause, S., Wilson, J.L., 2014. Effect of low-permeability layers on spatial patterns of hyporheic exchange and groundwater upwelling. Water Resources Research, 50(6): 5196-5215. DOI:10.1002/2013wr015054

Hantush, M.M., 2005. Modeling stream-aquifer interactions with linear response functions. Journal of Hydrology, 311(1-4): 59-79. DOI:10.1016/j.jhydrol.2005.01.007

Herzog, S.P., Ward, A.S., Wondzell, S.M., 2019. Multiscale Feature-feature Interactions Control Patterns of Hyporheic Exchange in a Simulated Headwater Mountain Stream. Water Resources Research, 55(12): 10976-10992. DOI:10.1029/2019wr025763

Hsieh, P.F., Yeh, H.D., 2014. Semi-analytical and approximate solutions for contaminant transport from an injection well in a two-zone confined aquifer system. Journal of Hydrology, 519: 1171-1176. DOI:10.1016/j.jhydrol.2014.08.046

Hu, H.Z. et al., 2019. Synthesized trade-off analysis of flood control solutions under future deep uncertainty: An application to the central business district of Shanghai. Water Res., 166: 13. DOI:10.1016/j.watres.2019.115067

Huang, C.S., Lin, W.S., Yeh, H.D., 2014. Stream filtration induced by pumping in a confined, unconfined or leaky aquifer bounded by two parallel streams or by a stream and an impervious stratum. Journal of Hydrology, 513: 28-44. DOI:10.1016/j.jhydrol.2014.03.039

Huang, C.S., Yeh, H.D., 2016. An analytical approach for the simulation of flow in a heterogeneous confined aquifer with a parameter zonation structure. Water Resources Research, 52(11): 9201-9212. DOI:10.1002/2016wr019443

Huang, Y.J. et al., 2020. Nature-based solutions for urban pluvial flood risk management. Wiley Interdiscip. Rev.-Water, 7(3): 17. DOI:10.1002/wat2.1421

Jeng, D.S., Li, L., Barry, D.A., 2002. Analytical solution for tidal propagation in a coupled semi-confined/phreatic coastal aquifer. Advances in Water Resources, 25(5): 577-584. DOI:10.1016/s0309-1708(02)00016-7

Krutz, L.J., Senseman, S.A., Zablotowicz, R.M., Matocha, M.A., 2005. Reducing herbicide runoff from agricultural fields with vegetative filter strips: a review. Weed Science, 53(3): 353-367. DOI:10.1614/ws-03-079r2

Lee, A., Aubeneau, A., Liu, X.F., Cardenas, M.B., 2021. Hyporheic Exchange in Sand Dunes Under a Freely Deforming River Water Surface. Water Resources Research, 57(3). DOI:10.1029/2020wr028817

Lee, A., Aubeneau, A.F., Cardenas, B., 2020. The Sensitivity of Hyporheic Exchange to Fractal Properties of Riverbeds. Water Resources Research, 56(5). DOI:10.1029/2019wr026560

Lewandowski, J. et al., 2019. Is the Hyporheic Zone Relevant beyond the Scientific Community? Water, 11(11). DOI:10.3390/w11112230

Li, H.L., Jiao, J.J., 2001. Analytical studies of groundwater-head fluctuation in a coastal confined aquifer overlain by a semi-permeable layer with storage. Advances in Water Resources, 24(5): 565-573. DOI:10.1016/s0309-1708(00)00074-9

Li, J., Chen, J.J., Zhan, H.B., Li, M.G., Xia, X.H., 2020. Aquifer recharge using a partially penetrating well with clogging-induced permeability reduction. Journal of Hydrology, 590. DOI:10.1016/j.jhydrol.2020.125391

Li, J., Zhan, H.B., Huang, G.H., You, K.H., 2011. Tide-induced airflow in a two-layered coastal land with atmospheric pressure fluctuations. Advances in Water Resources, 34(5): 649-658. DOI:10.1016/j.advwatres.2011.02.014

Li, X., Wen, Z., Zhan, H.B., Wu, F.X., Zhu, Q., 2021. Laboratory observations for two-dimensional solute transport in an aquifer-aquitard system. Environmental Science and Pollution Research, 28(29): 38664-38678. DOI:10.1007/s11356-021-13123-1

Liang, X.Y., Zhan, H.B., Schilling, K., 2018. Spatiotemporal Responses of Groundwater Flow and Aquifer-River Exchanges to Flood Events. Water Resources Research, 54(3): 1513-1532. DOI:10.1002/2017wr022046

Liang, X.Y., Zhan, H.B., Zhang, Y.K., Liu, J., 2017a. On the coupled unsaturated-saturated flow process induced by vertical, horizontal, and slant wells in unconfined aquifers. Hydrology and Earth System Sciences, 21(2): 1251-1262. DOI:10.5194/hess-21-1251-2017

Liang, X.Y., Zhan, H.B., Zhang, Y.K., Schilling, K., 2017b. Base flow recession from unsaturated-saturated porous media considering lateral unsaturated discharge and aquifer compressibility. Water Resources Research, 53(9): 7832-7852. DOI:10.1002/2017wr020938

Liang, X.Y., Zhang, Y.K., 2013. Analytic solutions to transient groundwater flow under time-dependent sources in a heterogeneous aquifer bounded by fluctuating river stage. Advances in Water Resources, 58: 1-9. DOI:10.1016/j.advwatres.2013.03.010

Liang, X.Y., Zhang, Y.K., Liu, J., Ma, E.Z., Zheng, C.M., 2019. Solute Transport With Linear Reactions in Porous Media With Layered Structure: A Semianalytical Model. Water Resources Research, 55(6): 5102-5118. DOI:10.1029/2019wr024778

Liang, X.Y., Zlotnik, V.A., Zhang, Y.K., Xin, P., 2020. Diagnostic Analysis of Bank Storage Effects on Sloping Floodplains. Water Resources Research, 56(2). DOI:10.1029/2019wr026385

Liu, D.S., Jiang, Q.H., Shi, W.Q., Chen, Q.W., Lee, J.Y., 2020. Hyporheic exchange mechanism driven by flood wave. Hydrological Processes, 34(26): 5429-5440. DOI:10.1002/hyp.13956

Lu, C.P. et al., 2020. Event-Driven Hyporheic Exchange during Single and Seasonal Rainfall in a Gaining Stream. Water Resources Management, 34(15): 4617-4631. DOI:10.1007/s11269-020-02678-2

Malama, B., Kuhlman, K.L., Barrash, W., Cardiff, M., Thoma, M., 2011. Modeling slug tests in unconfined aquifers taking into account water table kinematics, wellbore skin and inertial effects. Journal of Hydrology, 408(1-2): 113-126. DOI:10.1016/j.jhydrol.2011.07.028

McCallum, J.L., Shanafield, M., 2016. Residence times of stream-groundwater exchanges due to transient stream stage fluctuations. Water Resources Research, 52(3): 2059-2073. DOI:10.1002/2015wr017441

Monachesi, L.B., Guarracino, L., 2011. Exact and approximate analytical solutions of groundwater response to tidal fluctuations in a theoretical inhomogeneous coastal confined aquifer. Hydrogeology Journal, 19(7): 1443-1449. DOI:10.1007/s10040-011-0761-y

Naiman, R.J., Decamps, H., 1997. The ecology of interfaces: Riparian zones. Annual Review of Ecology and Systematics, 28: 621-658. DOI:10.1146/annurev.ecolsys.28.1.621

Neuman, S.P., 1972. Theory of flow in unconfined aquifers considering delayed response of water table. Water Resources Research, 8(4): 1031-+. DOI:10.1029/WR008i004p01031

Nilsson, C., Berggren, K., 2000. Alterations of riparian ecosystems caused by river regulation. Bioscience, 50(9): 783-792. DOI:10.1641/0006-3568(2000)050[0783:Aorecb]2.0.Co;2

Ou, Y., Wang, X.Y., Wang, L.X., Rousseau, A.N., 2016. Landscape influences on water quality in riparian buffer zone of drinking water source area, Northern China. Environmental Earth Sciences, 75(2). DOI:10.1007/s12665-015-4884-7

Pryshlak, T.T., Sawyer, A.H., Stonedahl, S.H., Soltanian, M.R., 2015. Multiscale hyporheic exchange through strongly heterogeneous sediments. Water Resources Research, 51(11): 9127-9140. DOI:10.1002/2015wr017293

Rathore, S.S., Lu, C.H., Luo, J., 2020. A Semianalytical Method to Fast Delineate Seawater-Freshwater Interface in Two-Dimensional Heterogeneous Coastal Aquifers. Water Resources Research, 56(9). DOI:10.1029/2020wr027197

Rumynin, V.G., Leskova, P.G., Sindalovskiy, L.N., Nikulenkov, A.M., 2019. Effect of depth-dependent hydraulic conductivity and anisotropy on transit time distributions. Journal of Hydrology, 579. DOI:10.1016/j.jhydrol.2019.124161

Saffi, M., 2014. Analytic solution to a one-dimensional, leaky, heterogeneous transient aquifer model. Hydrological Sciences Journal-Journal Des Sciences Hydrologiques, 59(1): 138-153. DOI:10.1080/02626667.2013.853120

Samani, N., Sedghi, M.M., 2015. Semi-analytical solutions of groundwater flow in multi-zone (patchy) wedge-shaped aquifers. Advances in Water Resources, 77: 1-16. DOI:10.1016/j.advwatres.2015.01.003

Sawyer, A.H., Cardenas, M.B., 2009. Hyporheic flow and residence time distributions in heterogeneous cross-bedded sediment. Water Resources Research, 45. DOI:10.1029/2008wr007632

Sawyer, A.H., Kaplan, L.A., Lazareva, O., Michael, H.A., 2014. Hydrologic dynamics and geochemical responses within a floodplain aquifer and hyporheic zone during Hurricane Sandy. Water Resources Research, 50(6): 4877-4892. DOI:10.1002/2013wr015101

Sedghi, M.M., Zhan, H.B., 2019. Groundwater flow to a general well configuration in an unconfined aquifer overlying a fractured bedrock. Journal of Hydrology, 575: 569-586. DOI:10.1016/j.jhydrol.2019.05.059

Sedghi, M.M., Zhan, H.B., 2021a. Groundwater flow to a well in a strip-shaped unconfined-fractured aquifer system with a transition zone. Journal of Hydrology, 596. DOI:10.1016/j.jhydrol.2021.126087

Sedghi, M.M., Zhan, H.B., 2021b. On Inflow to a Tunnel in a Fractured Double-Porosity Aquifer. Groundwater, 59(4): 562-570. DOI:10.1111/gwat.13079

Singh, S.K., 2004. Aquifer response to sinusoidal or arbitrary stage of semipervious stream. Journal of Hydraulic Engineering, 130(11): 1108-1118. DOI:10.1061/(asce)0733-9429(2004)130:11(1108)

Singh, T. et al., 2019. Dynamic Hyporheic Zones: Exploring the Role of Peak Flow Events on Bedform-Induced Hyporheic Exchange. Water Resources Research, 55(1): 218-235. DOI:10.1029/2018wr022993

Stehfest, H., 1970. Numerical inversion of laplace transforms. Communications of the Acm, 13(1): 47-&. DOI:10.1145/361953.361969

Su, X.R. et al., 2020. Scale issues and the effects of heterogeneity on the dune-induced hyporheic mixing. Journal of Hydrology, 590. DOI:10.1016/j.jhydrol.2020.125429

Sun, D.M., Zhan, H.B., 2007. Pumping induced depletion from two streams. Advances in Water Resources, 30(4): 1016-1026. DOI:10.1016/j.advwatres.2006.09.001

Talbot, A., 1979. Accurate numerical inversion of laplace transforms. Journal of the Institute of Mathematics and Its Applications, 23(1): 97-120.

Thorne, C.R., Tovey, N.K., 1981. Stability of composite river banks. Earth Surface Processes and Landforms, 6(5): 469-484. DOI:10.1002/esp.3290060507

Vandegiesen, N.C., Parlange, J.Y., Steenhuis, T.S., 1994. Transient flow to open drains - comparison of linearized solutions with and without the dupuit assumption. Water Resources Research, 30(11): 3033-3039. DOI:10.1029/94wr01733

Wang, Q.R., Zhan, H.B., Tang, Z.H., 2015. Two-dimensional flow response to tidal fluctuation in a heterogeneous aquifer-aquitard system. Hydrological Processes, 29(6): 927-935. DOI:10.1002/hyp.10207

Ward, A.S., Gooseff, M.N., Johnson, P.A., 2011. How can subsurface modifications to hydraulic conductivity be designed as stream restoration structures? Analysis of Vaux's conceptual models to enhance hyporheic exchange. Water Resources Research, 47. DOI:10.1029/2010wr010028

Wu, H.Q., Lu, C.H., Yan, M., Werner, A.D., 2020. Expanding Freshwater Lenses Adjacent to Gaining Rivers Through Vertical Low-Hydraulic-Conductivity Barriers: Analytical and Experimental Validation. Water Resources Research, 56(2). DOI:10.1029/2019wr025750

Xu, H.Q. et al., 2022. Compound flood impact of water level and rainfall during tropical cyclone periods in a coastal city: the case of Shanghai. Nat. Hazards Earth Syst. Sci., 22(7): 2347-2358. DOI:10.5194/nhess-22-2347-2022

Yeh, H.D., Kuo, C.C., 2010. An analytical solution for heterogeneous and anisotropic anticline reservoirs under well injection. Advances in Water Resources, 33(4): 419-429. DOI:10.1016/j.advwatres.2010.01.007

Zakian, V., 1969. Numerical inversion of laplace transform. Electronics Letters, 5(6): 120-&. DOI:10.1049/el:19690090

Zhan, H.B., Zlotnik, V.A., 2002. Groundwater flow to a horizontal or slanted well in an unconfined aquifer. Water Resources Research, 38(7). DOI:10.1029/2001wr000401

Zlotnik, V.A., Huang, H., 1999. Effect of shallow penetration and streambed sediments on aquifer response to stream stage fluctuations (analytical model). Ground Water, 37(4): 599-605. DOI:10.1111/j.1745-6584.1999.tb01147.x

Table 1. Review of analytical model considering heterogeneity of aquifer.

	Research	Heterogeneity	Dimension	Type of aquifer	Driver force
1	Monachesi and Guarracino, 2011	linear increase K	1D	confined	sea
2	Chuang et al., 2010	n vertical layers	1D	confined	sea
3	Wang et al., 2015	linear increase K	2D	confined	sea
4	Li et al., 2011	2 layers	1D	unconfined	sea
5	Li and Jiao, 2001	2 layers	2D	confined	sea
6	Jeng et al., 2002	2 layers	2D	unconfined	sea
7	Rathore et al., 2018	n layers	2D	confined	sea
8	Rathore et al., 2020	2D field	2D	confined	sea
9	Liang and Zhang, 2013	n vertical layers	1D	unconfined	river and recharge
10	Huang and Yeh, 2016	n vertical layers	2D	confined	river and well
11	Rumynin et al., 2019	exponential decay K	2D	confined	river and recharge
12	Butler et al., 2008	2 layers	3D	unconfined	well and river
13	Samani and Sedghi, 2015	2 layers	3D	unconfined	well
14	Feng et al., 2021	3 layers	2D	confined	well
15	Feng et al., 2020	3 layers	2D	confined	well
16	Feng et al., 2019	2 layers	2D	confined	well
17	Yeh and Kuo, 2010	2 layers	2D	confined	well
18	Avci and Sahin, 2014	n vertical layers	1D	confined	well
19	Sedghi and Zhan, 2019	2 layers	3D	unconfined	well
20	Sedghi and Zhan, 2021	3 vertical layers	3D	unconfined	well
21	Chang et al., 2008	n vertical layers	1D	unconfined	diriclet boundary and recharge
22	Saffi, 2014	2 vertical layers	1D	confined	leaky
23	Present solution	2 layers	2D	unconfined	river and recharge

Table 2. Definition of dimensionless variables.

$h_{1D} = \frac{h_1}{h_0}$	$h_{2D} = \frac{h_2}{h_0}$
$x_D = \frac{x}{L}$	$z_D = \frac{z}{L}$
$B_{1D} = \frac{B_1}{L}$	$B_{2D} = \frac{B_2}{L}$
$K_x = \sqrt{K_{x1}K_{x2}}$	$S_S = \sqrt{S_{s1}S_{S2}}$
$t_D = \frac{K_x t}{S_s L^2}$	$R_K = \frac{K_{x2}}{K_{x1}}$
$R_S = \sqrt{\frac{S_{s2}}{S_{s1}}}$	$K_{1D} = \frac{K_{z1}}{K_{x1}}$
$K_{2D} = \frac{K_{z2}}{K_{x2}}$	$H_{bD} = \frac{H_b}{H_0}$
$W_D = \frac{WL}{K_x H_0}$	$S_{yD} = \frac{S_y}{S_s L}$
$R_v = \frac{K_{1D}}{K_{2D} R_K^2}$	$Q_D = \frac{Q}{h_0 K_x}$
$Q_{1D} = \frac{Q_1}{h_0 K_x}$	$Q_{2D} = \frac{Q_2}{h_0 K_x}$

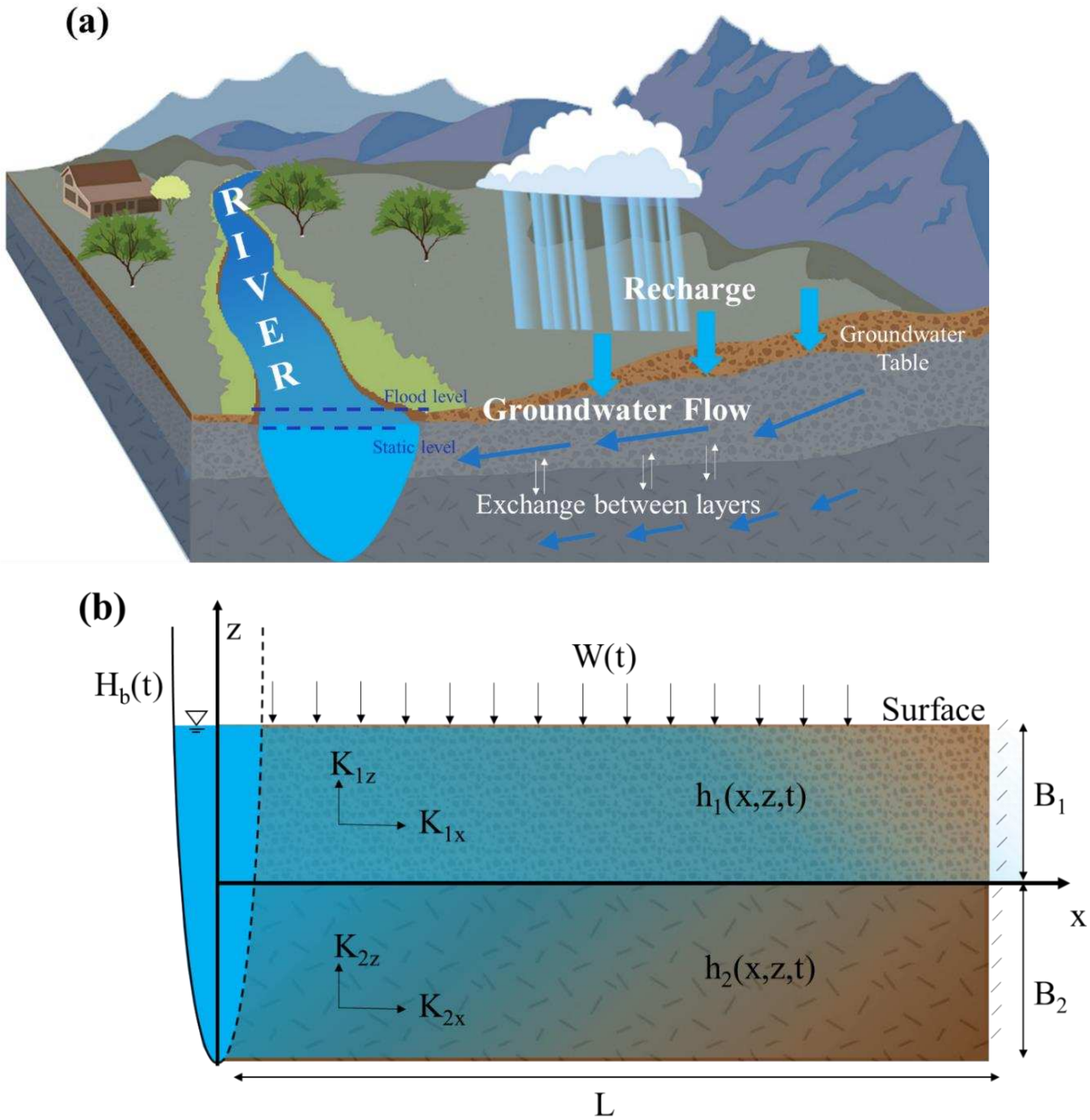

Figure 1. (a) Schematic diagram of groundwater flow in a layered aquifer; (b) conceptual model of groundwater flow to a river in an unconfined aquifer with two-layer porous media.

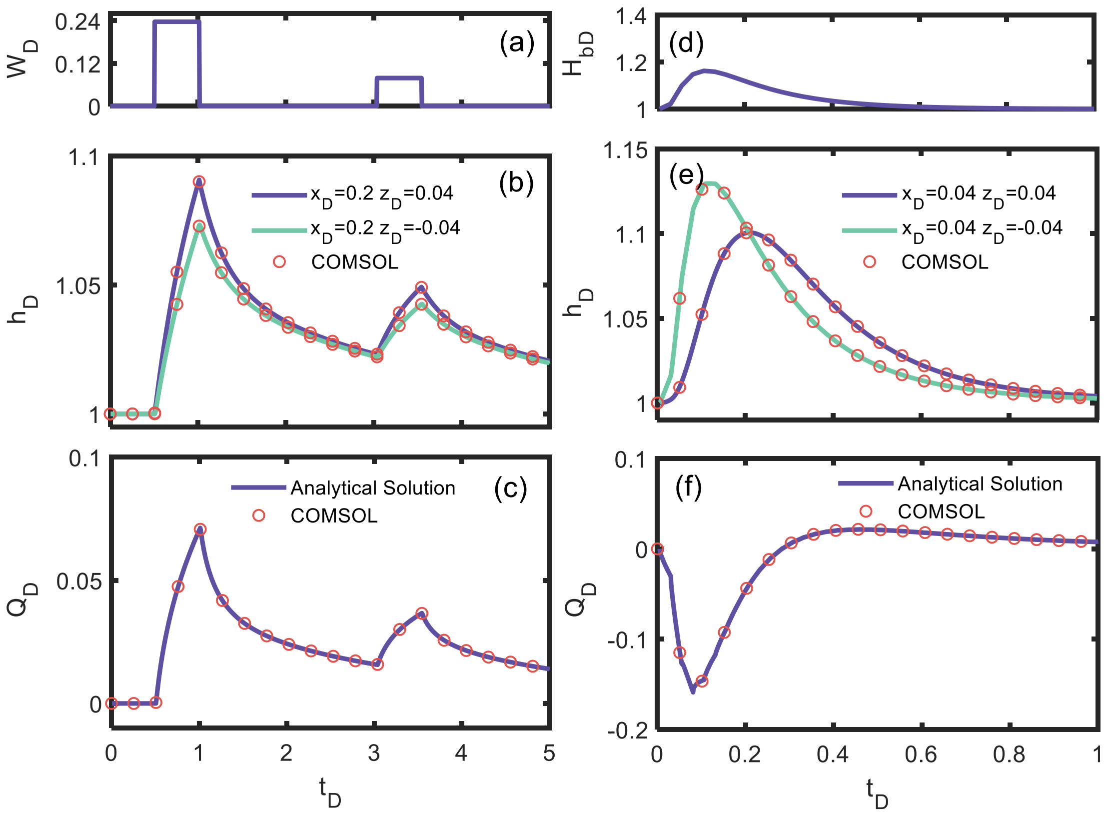

Figure 2. Comparison of the analytical solutions (solid curves) and the numerical solutions (open circles) for two recharge events (left column) and a flood event (right column): (a) the dimensionless recharge W_D against dimensionless time t_D; (b) the dimensionless hydraulic head h_D against t_D at two locations; (c) the dimensionless discharge Q_D against t_D. For the right column: (d) the dimensionless river stage H_{bD} against t_D; (e) h_D against t_D at two locations; (f) Q_D against t_D.

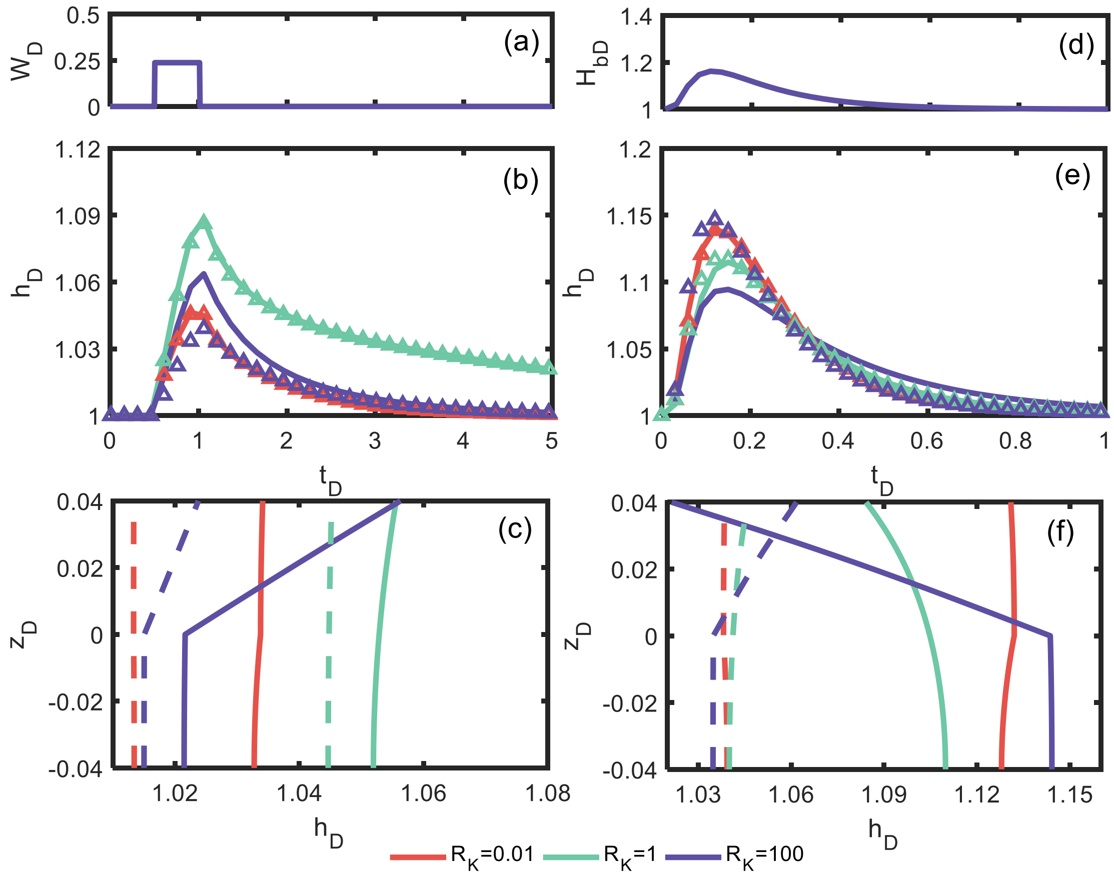

Figure 3. Responses of the dimensionless hydraulic heads to the recharge event (left column) and the flood event (right column) for the different R_K (0.01, 1, and 100). For the left column: (a) the dimensionless recharge W_D against time t_D; (b) the dimensionless hydraulic head h_D against t_D at the upper layer (x_D=0.2, z_D=0.02, solid curves) and the lower layer (x_D=0.2, z_D=-0.02, triangle curves); (c) the vertical profiles of h_D for the different times (t_D=0.75, solid curves and t_D=2, dashed curves). For the right column: (d) the dimensionless river stage H_{bD} against t_D; (e) h_D against t_D at the upper layer (x_D=0.04, z_D=0.02, solid curves) and the lower layer (x_D=0.04, z_D=-0.02, triangle curves); (f) the vertical profiles of h_D for the different times (t_D=0.1, solid curves and t_D=0.4, dashed curves).

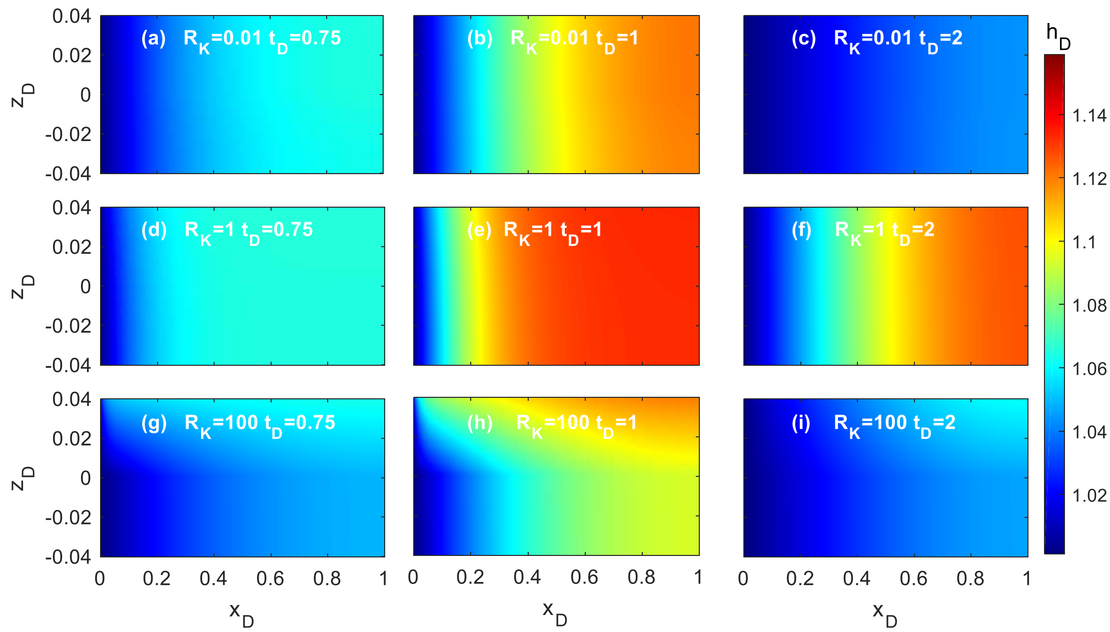

Figure 4. Vertical profiles of the dimensionless hydraulic heads induced by the recharge event for the different R_K (0.01, 1, and 100) at different dimensionless times t_D (0.75, 1, and 2).

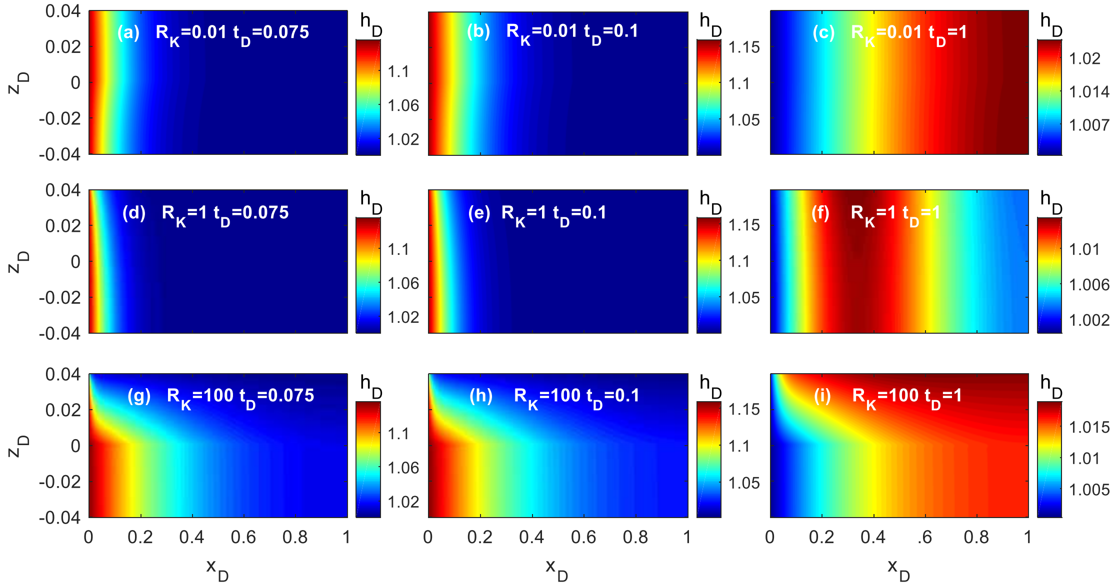

Figure 5. Vertical profiles of the dimensionless hydraulic heads induced by the flood event for the different R_K (0.01, 1, and 100) at different dimensionless times t_D (0.075, 0.1, and 1).

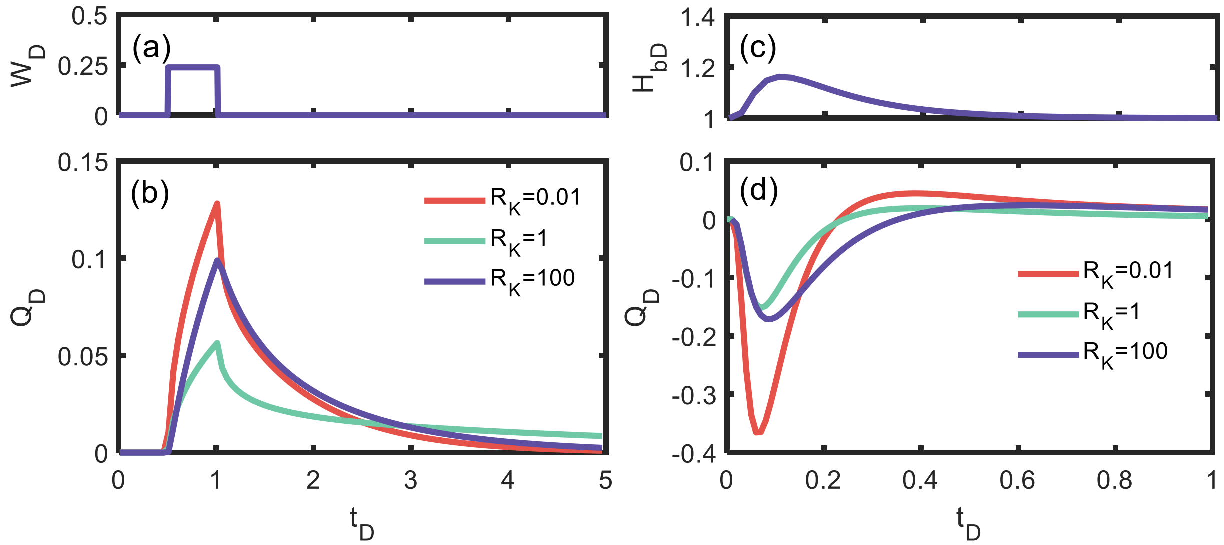

Figure 6. Responses of the dimensionless lateral discharge Q_D to the recharge event (left column) and the flood event (right column) for the different R_K (0.01, 1, and 100). For the left column: (a) the recharge W_D against dimensionless time t_D; (b) the dimensionless discharge Q_D against t_D. For the right column: (c) the river stage H_{bD} against t_D; (d) the dimensionless discharge Q_D against t_D.

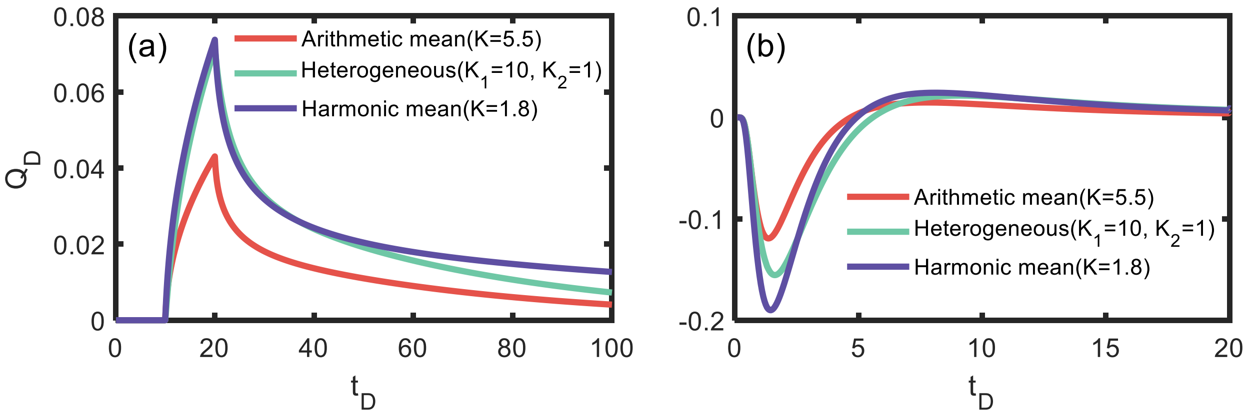

Figure 7. Responses of the discharge Q to the recharge event (a) and the flood event (b) for the arithmetic mean, heterogeneous hydraulic conductivity, and harmonic mean. (a) The dimensionless discharge Q_D against dimensionless time t_D in the recharge event; (b) the dimensionless discharge Q_D against t_D in the flood event.

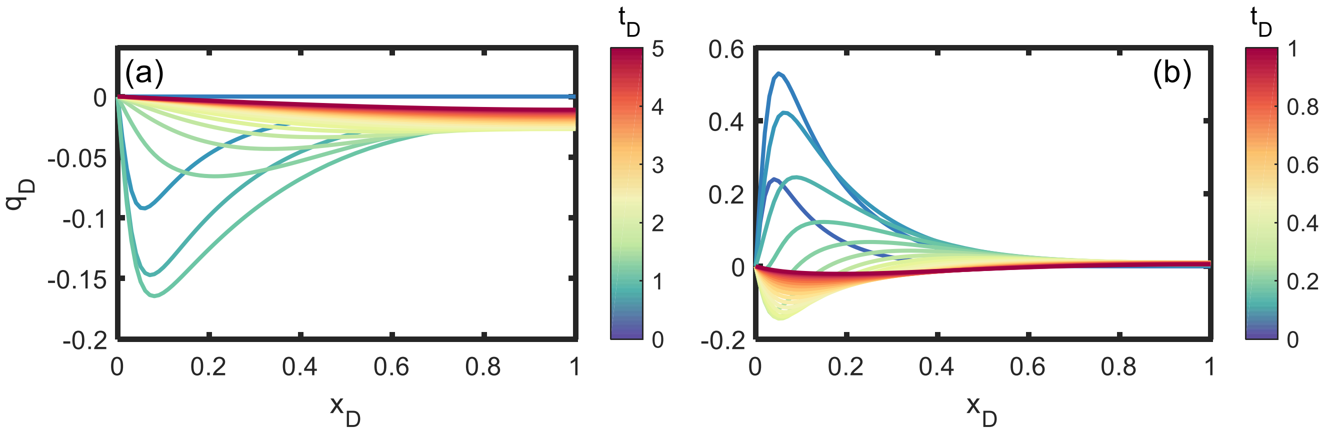

Figure 8. Distributions of dimensionless exchange flux across the interface of the two zones along the x - direction at different times in the recharge event (a) and the flood event (b).

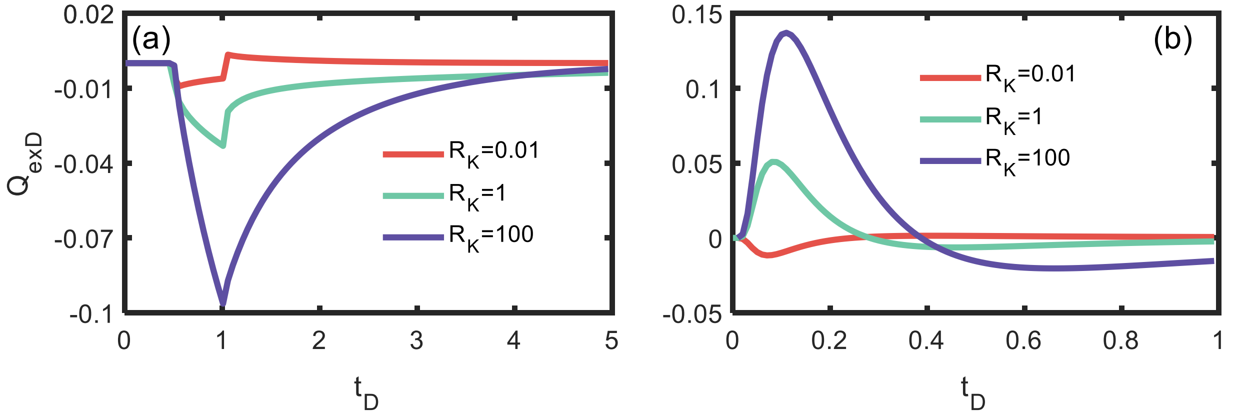

Figure 9. Response of dimensionless total exchange flux Q_{exD} to the recharge event (a) and the flood event (b) for different values of R_x. (a) The dimensionless total exchange flux Q_{exD} against dimensionless time t_D in the recharge event; (b) the dimensionless total exchange flux Q_{exD} against t_D in the flood event.

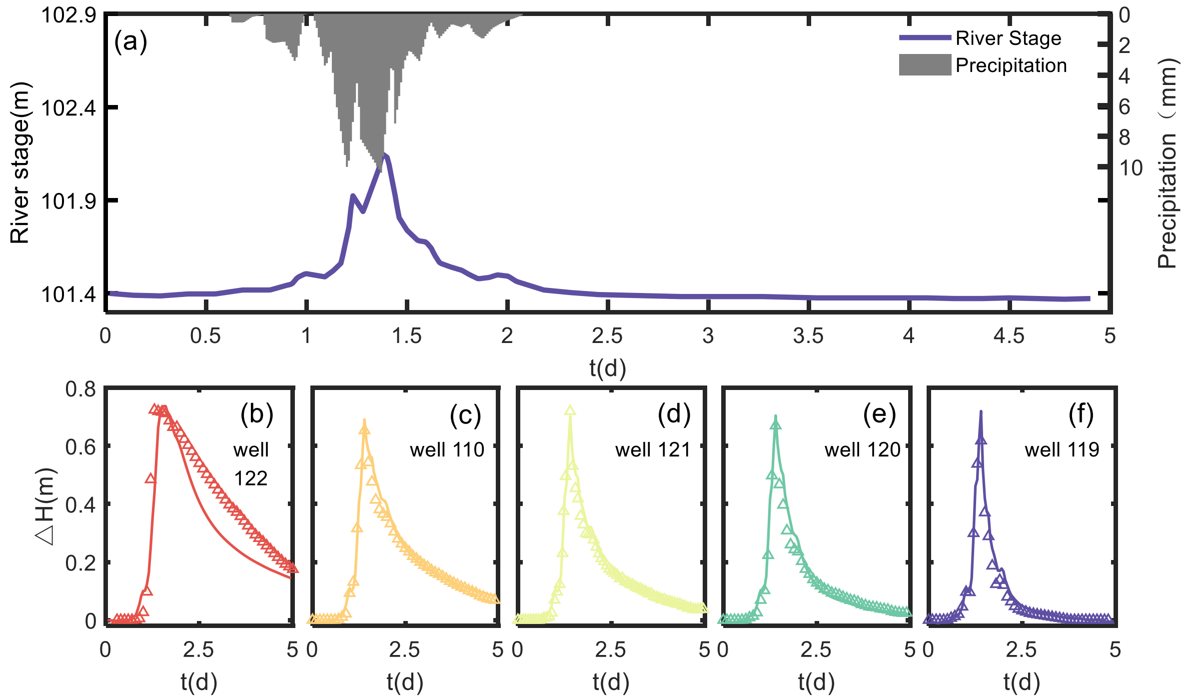

Figure 10. Field data observed by Sawyer et al. (2014) and the analytical model solutions. (a) The observed precipitation and river stage against time (t); the comparison between the analytical model solutions and the change of observed hydraulic head (ΔH) against time (t) for well 122 (b), well 110 (c), well 121 (d), well 120 (e) and well 119 (f). Solid colored lines represent analytical solutions, and colored triangles represent field data.

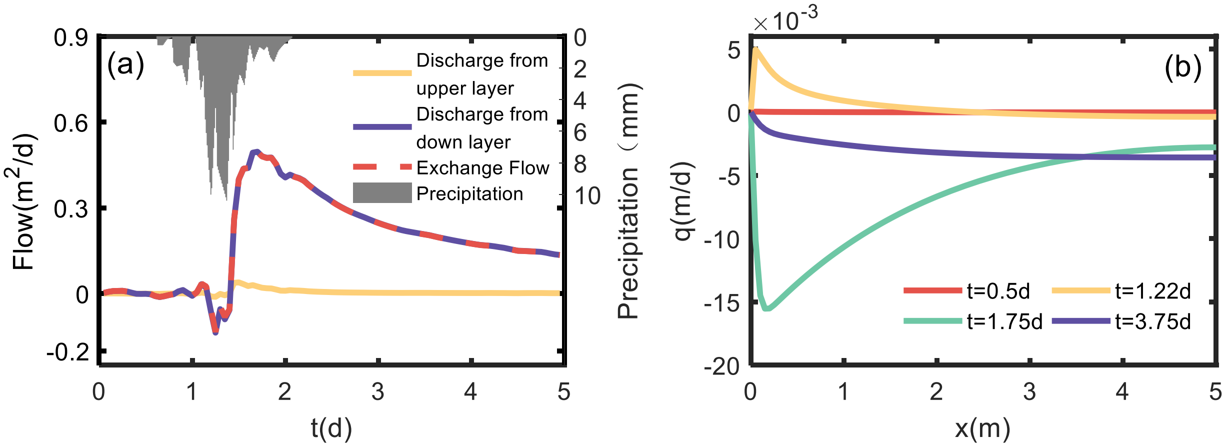

Figure 11. The effect of the two-layer structure on the hyporheic flow mechanism. (a) The precipitation, total exchange flow between two layers, discharge from the bottom layer, and discharge from the upper layer; (b) exchange flow between two layers at specific times.